






Assessing the Accuracy of Machine Learning Thermodynamic Perturbation Theory: Density Functional Theory and Beyond

Basile Herzog ^{a,†}, Maurício Chagas da Silva ^{b,†}, Bastien Casier [†], Michael
Badawi [†], Fabien Pascale,[†] Tomáš Bučko ^{*,‡,¶}, Sébastien Lebègue,[†] and Dario
Rocca ^{*,†}

[†]*Université de Lorraine and CNRS, Laboratoire de Physique et Chimie Théorique, UMR
7019, 54506, Vandœuvre-lès-Nancy, France*

[‡]*Comenius University in Bratislava, Department of Physical and Theoretical Chemistry,
Faculty of Natural Sciences, Mlynská Dolina, Ilkovičova 6, SK-84215 Bratislava, Slovakia*

[¶]*Institute of Inorganic Chemistry, Slovak Academy of Sciences, Dúbravská cesta 9,
SK-84236 Bratislava, Slovakia*

E-mail: tomas.bucko@uniba.sk; dario.rocca@univ-lorraine.fr

^aShared first authorship: BH and MCS contributed equally to this work

^bShared first authorship: BH and MCS contributed equally to this work

Abstract

Machine learning thermodynamic perturbation theory (MLPT) is a promising approach to compute finite temperature properties when the goal is to compare several different levels of *ab initio* theory and/or to apply highly expensive computational methods. Indeed, starting from a production molecular dynamics trajectory, this method can estimate properties at one or more target levels of theory from only a small number of additional fixed-geometry calculations, which are used to train a machine learning model. However, as MLPT is based on thermodynamic perturbation theory (TPT), inaccuracies might arise when the starting point trajectory samples a configurational space which has a small overlap with that of the target approximations of interest. By considering case studies of molecules adsorbed in zeolites and several different density functional theory approximations, in this work we assess the accuracy of MLPT for ensemble total energies and enthalpies of adsorption. The problematic cases that were found are analyzed and it is shown that, even without knowing exact reference results, pathological cases for MLPT can be detected by considering a coefficient that measures the statistical imbalance induced by the TPT reweighting. For the most pathological examples we recover target level results within chemical accuracy by applying a machine learning-based Monte Carlo (MLMC) resampling. Finally, based on the ideas developed in this work, we assess and confirm the accuracy of recently published MLPT-based enthalpies of adsorption at the random phase approximation level, whose high computational cost would completely hinder a direct molecular dynamics simulation.

1 Introduction

Correlated quantum chemical methods could provide an alternative to density functional theory (DFT) in (periodic) materials simulations possibly reaching the threshold of chemical accuracy (1 kcal/mol) with respect to experimental data. Traditional quantum chemical methods, such as Møller-Plesset perturbation theory to second order (MP2)¹ or coupled-cluster theory², have been recently implemented for condensed phase materials applications³⁻⁷. An alternative particularly suitable for condensed matter applications is represented by the random phase approximation (RPA)⁸⁻¹⁴ and its variants which include higher order corrections¹⁵⁻²¹. Due to the significantly high computational cost of these approaches, their use is limited, especially in (finite-temperature) molecular dynamics (MD) simulations.

The use of machine learning (ML) techniques could be highly beneficial for MD simulations and, since the seminal work of Behler and Parrinello (BP) in 2007²², has seen an increasing popularity in this field²³⁻²⁶. While keeping a level of accuracy comparable to *ab initio* calculations, ML approaches can be used to replace most of the expensive quantum mechanical calculations with numerically cheap predictions. This allows for an increase in the system size and timescale that would be normally accessible by traditional *ab initio* MD simulations. However, ML models typically employed in MD simulations require a significant amount of data to be trained and this represents an issue for the most expensive quantum mechanical approximations.

In a recent work, some of us applied a scheme that couples machine learning techniques with thermodynamic perturbation theory (MLPT) to compute enthalpies of adsorption of molecules in the zeolite chabazite at the RPA level of theory²⁷ (the same methodology can be used in the context of free energies of activation^{28,29}). Achieving these results with a brute force molecular dynamics simulation would be completely out of reach. Indeed, by considering only the cost of the RPA energy calculations for the zeolite, completing a 200000

steps MD simulation would require 65M CPU hours and more than 110 years on 64 cores at 2.6 GHz (this estimate does not include the significant additional cost of computing RPA forces³⁰). With our MLPT technique as few as 10 single point RPA energy calculations were sufficient to train a machine learning model that was then used to predict the RPA energy for several other configurations²⁷.

In this previous work the van der Waals (vdW) corrected PBE+D2 functional^{31,32} was used to generate a production MD trajectory (in general, a numerically inexpensive approximation should be chosen as production method). Based on the Δ -ML method³³, a model was thereafter trained to predict the difference between RPA and PBE+D2 energies. Following the thermodynamic perturbation approach³⁴⁻³⁶ the energy differences were subsequently used to reweight the statistical weight of the PBE+D2 configurations in order to obtain the RPA canonical distribution and compute the RPA ensemble energies and enthalpies (in this context the RPA is considered the “target” level of theory). Thanks to the inexpensive predictions of the ML model, this technique involves a computational cost that is several orders of magnitude smaller than a full RPA MD simulation.

While the error involved in the ML procedure is rather well controlled^{27,28}, the application of thermodynamic perturbation theory (TPT) might be at the origin of a bias in the results estimated at the target level of theory. Indeed, the configurational space sampled by the production MD might have suboptimal superposition with the target configurational space^{34,35}. In certain cases this might lead to a strong loss of statistical significance when the contributions of the production configurations are reweighted to obtain the target distribution (namely only few configurations could contribute to the whole target level statistics).

In this work, we assess the accuracy of the MLPT approach using the adsorption of molecules in zeolites as a test case. Indeed, many separation and adsorption processes re-

quire the improvement of the dedicated materials, and DFT calculations often provide suitable suggestions of optimized formulations in this regard³⁷⁻⁴⁰. However, additional efforts have to be done to find a better compromise between accuracy of prediction and calculation cost. By considering five different DFT functionals, including generalized gradient approximation (GGA), meta-GGA, and non-local vdW corrected functionals, we perform full MD simulations to provide “exact” reference values for the ensemble energies and enthalpies of adsorption. We then use each one of these five functionals as a production method and apply MLPT to obtain the energy/enthalpy estimates for the remaining four functionals, which are considered as target approximations.

By comparing MLPT estimates with exact reference results the level of accuracy of this approach is established. Some pathological cases are found, for example when GGA functionals are used as starting point for meta-GGA functionals and vice versa (in certain cases the MLPT estimate of the ensemble energy can deviate by more than 8 kcal/mol). By using machine learning dimensionality reduction algorithms, we qualitatively visualize the relative distributions of the configurations from the different MD simulations. This analysis confirms that the most problematic cases can be ascribed to a poor superposition of the configurational spaces. In order to detect possible failure of MLPT we propose a diagnostic test, the I_w index, which is evaluated from ML energy predictions and does not rely on the knowledge of any exact reference results.

We then propose a scheme to significantly improve results even when the I_w coefficient is close to 0 (lowest production-target superposition). This approach, denoted as MLMC, is based on a Monte Carlo resampling of the target configurational space that reuse the machine learning model already trained for MLPT. Without any additional target level calculations this scheme decreases even the largest deviations within the threshold of chemical accuracy.

Finally, we apply the tools developed in this work to analyze our previous results based on the RPA²⁷, where reference values cannot be produced. The relatively large values of the I_w index hints that the PBE+D2 functional provides a reliable starting point for RPA target properties. The results are stable even if a full MLMC resampling of the configurational space is performed. This shows that, with a proper choice of the production approximation, MLPT allows for a quick and accurate estimate of target level properties. The MLPT approach opens the way to a more systematic application of accurate but expensive DFT and quantum chemical approximations in finite temperature simulations of materials.

The layout of the paper is organized as follows. In the following section, Sec. 2, we discuss the methodological part of this work and provide computational details. In Sec. 3, we present numerical results and analyze them. Sec. 4 contains our conclusions.

2 Methodology

The enthalpies of adsorption ($\Delta_{ads}H$) of the CH_4 molecule in protonated chabazite (HCHAB) and CO_2 molecule in siliceous chabazite (SiCHAB) were investigated by employing *ab initio* molecular dynamics (AIMD) and machine learning thermodynamic perturbation theory^{27–29} (MLPT). The models of the adsorbed molecules are shown in **Fig. (1)**. The enthalpy of adsorption is defined by

$$\Delta_{ads}H(M@Z) = \langle E(M@Z) \rangle - (\langle E(M) \rangle + \langle E(Z) \rangle) - k_B T \quad (1)$$

where $\langle E \rangle$ is the internal energy computed as ensemble average of potential energy via the AIMD simulations or MLPT (M denotes the molecules, Z the zeolites, and M@Z the adsorbed system), k_B is the Boltzmann constant, and T is the system temperature (equal to 300K in all our simulations).

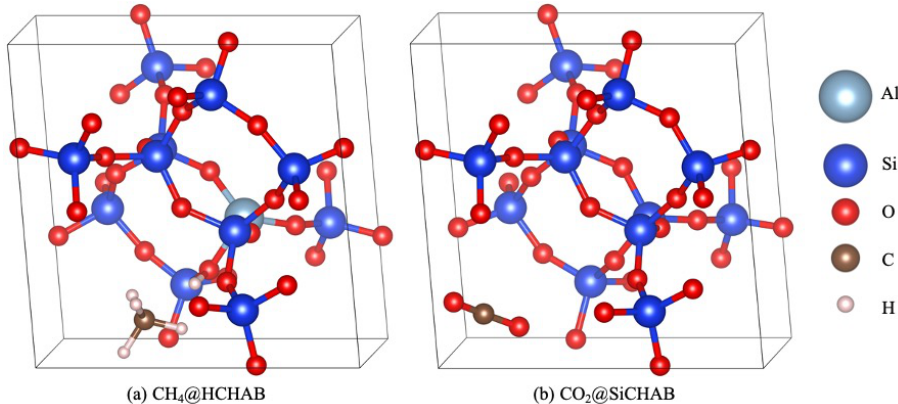


Figure 1: (a) CH_4 in protonated Chabazite (HCHAB) and (b) CO_2 in siliceous chabazite (SiCHAB).

The goal of this work is to benchmark the accuracy of MLPT by comparing its estimates with “exact” reference values obtained from full MD simulations. We chose five DFT functionals in order to span a range of different characteristics but keeping also into account their numerical cost, as long and stable MD trajectories have to be produced for reference.

Specifically, we selected: a generalized gradient approximation (GGA) functional, PBE⁴¹ and its version with corrections for van der Waals interactions, PBE+D2^{31,32}; a meta-GGA functional, SCAN^{42,43}; a non-local vdW functional, vdW-DF2^{44,45}; a version of SCAN with non-local vdW corrections, SCAN+rVV10⁴⁶. We will also discuss results based on the random phase approximation (RPA), as implemented in the VASP code⁴⁷⁻⁴⁹; due to the high numerical cost a direct MD simulation at this level of theory is completely out of reach and the MLPT method becomes instrumental to estimate finite temperature properties.

All AIMD simulations were performed within the NVT ensemble, whereby temperature was maintained by Andersen⁵⁰ thermostat with collision probability of 0.05. An integration time step of 0.5 fs was considered and the total simulation time of each MD run was 100 ps, i.e. $\sim 200 \cdot 10^3$ configurations were generated with each method for each system investigated in this work. The initial part of 10 ps of each trajectory was considered as an equilibration period and the corresponding data were discarded. The remaining part of the trajectory was tested for the absence of any drift via Mann-Kendall tests⁵¹. All the standard errors on the ensemble energies of these trajectories are below 0.2 kcal/mol.

In the AIMD simulations we used a cell fixed at the lattice parameters of the chabazite optimized at the PBE level ($a = b = c = 9.34 \text{ \AA}$ and $\alpha = \beta = \gamma = 95^\circ$). All AIMD simulations as well as single point calculations were carried out with the VASP electronic structure package^{13,47-49}. PAW pseudopotentials⁵² for all atoms with the default kinetic energy cutoffs were used to expand the wavefunctions. The “accurate” precision setting was used and the hydrogen atomic mass was increased to 3.0 a.u. The Γ point approximation was applied in all calculations.

The results produced by AIMD are used as a reference for our MLPT method. Within this approach an MD simulation is first performed at a certain production level of theory

and then “corrected” to obtain results at one or multiple target levels of theory. One of the advantages of MLPT is that an estimate of a finite-temperature property for the target method can be obtained with only a few tens or few hundreds of single point calculations²⁷. Out of about $1900 \cdot 10^3$ configurations generated in production runs, a reduced sample of about $19 \cdot 10^3$ evenly separated configurations (X_i) and corresponding potential energies obtained with the production method (E_i) are selected to be used for the predictions of the energies at the new target functional level. We note that this configuration reduction is not strictly necessary but, since MD configurations close in time are correlated, this procedure speeds up the predictions of the ML model without compromising the accuracy of prediction.

In order to compute target level ensemble energies $\langle E' \rangle$, MLPT applies TPT to reweight the production statistical distribution³⁵

$$\langle E' \rangle = \frac{\sum_i^M E'_i \exp(-\beta \Delta E_i)}{\sum_i^M \exp(-\beta \Delta E_i)} \quad (2)$$

where E'_i denotes the target level energies of the i th configuration, $\Delta E_i = E'_i - E_i$ is the difference between target and production energies, $\beta = 1/k_B T$, and M is the number of configurations, in this case $19 \cdot 10^3$.

The application of **Eq. (2)** still requires a large number (M) of calculations at the target level of theory. In MLPT only a very small number N_{train} of these calculations is actually performed and then used to train an ML model that predicts all the remaining $M - N_{train}$ energies. This procedure has been described in detail in Ref.²⁷ and here we will only summarize the main technical points. In order to decrease the number of target calculations required to train the ML algorithm instead of considering directly the target energy E'_i , we build a ML regression model using ΔE_i . This approach, which is just one of the many possible applications of the Δ -ML idea^{33,53}, takes advantage of the much smoother dependence of ΔE_i on E_i in comparison with E'_i and, accordingly, is easier to predict. To represent

the configurations within our ML model we use the *Smooth Overlap of Atomic Positions* (SOAP)⁵⁴ descriptor, as implemented in the Dscribe library⁵⁵. While several other descriptors for periodic materials have been proposed in the literature⁵⁶⁻⁵⁸, the choice of the SOAP descriptor provides already a satisfactory level of accuracy for MLPT applications²⁷⁻²⁹.

The SOAP approach leads to a natural definition of a kernel for local atomic environments that can be subsequently used to define the global rematch kernel⁵⁹. This kernel, which can be intuitively seen as a measure of similarity between configurations, is then used in the framework of the kernel ridged regression (KRR)⁵⁹ ML algorithm; the KRR implementation in the Scikit-learning package is used in this work⁶⁰. To train the ML model, 200 evenly distributed configurations are chosen from the $19 \cdot 10^3$ structures of the production trajectory. An additional independent set of 25 configurations is also selected to test the accuracy of the predictions of the ML model; for all the applications considered in this work the root mean square error (RMSE) in the prediction of the energy of single configurations is at most 0.3 kcal/mol. Single point calculations at the target level are performed exclusively for these 225 configurations. The 18775 (i.e., 19000-225) remaining values of ΔE_i (and $E'_i = E_i + \Delta E_i$) necessary to evaluate **Eq. (2)** are inexpensively predicted by the ML model. This shows the clear advantage of using MLPT, in particular if it is necessary to consider multiple target level theories or highly expensive approximations (e.g., the RPA).

As discussed in the next sections MLPT does not provide satisfactory results in certain cases. This happens for the estimate of SCAN and SCAN+rVV10 adsorption enthalpies from PBE production calculations. This issue is related to the unsatisfactory superposition of the target and production configurational spaces. To improve the results in these cases we have reused the ML model from the MLPT application to resample the target level configurational space using the Monte Carlo (MC) algorithm⁶¹⁻⁶⁴. We will denote this procedure as MLMC.

The MC approach used to sample the canonical ensemble is equivalent to MD but is simpler to implement and does not require the calculation of forces (for certain methods forces are not available in most solid state physics software implementations). By using our in-house software, the MLMC approach recursively sample new configurations following these steps: (1) A new geometric configuration is randomly generated; (2) A production level *ab initio* calculation is performed to obtain E_i for this new configuration; (3) the ML learning model is used to predict ΔE_i and E'_i ; (4) the new configuration is accepted or rejected according to the Metropolis criterion⁶¹⁻⁶⁴. The advantage of MLMC is that with respect to MLPT no additional calculations are required at the target level of theory and this is particularly important when computationally expensive quantum chemical methods are used. The trade-off is that each step of the MC procedure requires a new production level calculation. In the applications of next section we have sampled $400 \cdot 10^3$ steps for each MLMC trajectory to get converged ensemble statistics (for all the systems considered in this work the standard error on the MC ensemble energies is at most 0.3 kcal/mol).

3 Results and Discussions

3.1 Assessing the accuracy of MLPT for different density functional approximations

The experimentally measured enthalpies of adsorption of the investigated systems are rather small, -4.06 kcal/mol and -5.02 kcal/mol for CH₄@ HCHAB and CO₂@ SiCHAB, respectively. Indeed, for both systems, the adsorption process is dominated by weak long-range van der Waals (vdW) interactions, which are, due to the small size of both adsorbate molecules, only modest. Ideally, very accurate methods such as RPA, MP2 or CCSD would be necessary to model with systematic improvements in accuracy such processes in which long-range interactions play an important role. While the use of such methods is prohibitive due to their enormous computational cost, machine learning techniques could play an important role in extending their applicability to realistic systems²⁷. This requires ML techniques that reasonably preserve the accuracy of these high-level quantum chemical methods and have sufficient predictive power for configurations beyond the training set. In this section we will discuss the accuracy of MLPT for the case of computationally affordable DFT functionals, for which an “exact” reference can be easily obtained. At the end of this section we will consider the RPA enthalpies of adsorption.

In **Table (1)**, we report the values of the enthalpies of adsorption (**Eq. (1)**) for CH₄ and CO₂ in zeolite as obtained from the full MD simulations. These results will be used as reference values for assessing the quality of our MLPT methodology. Comparing the calculated and the experimental values for the enthalpies of adsorption in **Table (1)**, it can be noticed that only functionals with some vdW corrections can achieve a reasonable agreement with the experimental values, although the accuracy improvement is not systematic. For the CH₄@HCHAB system, SCAN+rVV10 was identified as the best performing functional, with a deviation of -0.71 kcal/mol (17% of deviation), whereas for the CO₂@SiCHAB the

best functional was PBE+D2 with a deviation of -0.46 kcal/mol (9% of deviation). On the other hand, the uncorrected PBE and SCAN functionals show a sizable underestimation in the calculated enthalpies of adsorption for the CH₄ and CO₂ molecules in the zeolites, with relative errors with respect to experiment higher than 35%. However, the main purpose of this work is not to compare the accuracy of different functionals compared to experiment but to assess the performance and limitations of MLPT to reproduce exact AIMD results obtained using different quantum mechanical approximations.

Table 1: Experimental and reference theoretical enthalpies of adsorption for the CH₄ and CO₂ molecules in zeolites obtained using different functionals. All values are expressed in kcal/mol.

System	PBE	PBE+D2	SCAN	vdW-DF2	SCAN+rVV10	Exp.
CH ₄ @HCHAB	-1.13	-6.08	-2.60	-5.64	-4.77	-4.06 ⁶⁵
CO ₂ @SiCHAB	-1.18	-5.48	-2.95	-6.93	-7.11	-5.02 ⁶⁶

Starting from each of the 5 trajectories obtained using PBE, PBE+D2, SCAN, vdW-DF2, and SCAN+rVV10 production methods, the MLPT approach is used to predict the results for all remaining approximations. The results are shown in **Table (2)**. In this table, columns and lines represent the production and target methods, respectively. If, for example, we consider the PBE column (below Production - MD simulations), and the SCAN line, we find an estimate of the SCAN enthalpy of adsorption that is obtained by applying MLPT to the PBE production trajectory; this estimate avoids completely the generation of a new SCAN molecular dynamics trajectory and requires only 200 additional SCAN calculations that are used to train the ML model. For the sake of completeness, we also report values on the diagonal of this table, namely MLPT values based on the same production and target levels of theory. This shows that some small fluctuations can be introduced by the ML model even in this particularly simple case, additionally to those regular/general fluctuations due

to the AIMD convergence and statistical uncertainty.

The accuracy of the MLPT estimates can be established by comparing the MLPT results with reference values of **Table (1)**. The corresponding deviations are reported in parenthesis in **Table (2)**. Altogether, it can be noticed that the predictions within the PBE/PBE+D2/vdW-DF2 group and the SCAN/SCAN+rVV10 are reasonable with deviations typically within few tens of kcal/mol and only in one case slightly beyond chemical accuracy (a deviation of 1.01 kcal/mol for the prediction of SCAN+rVV10 from SCAN for CO₂@SiCHAB). When the production and target methods belong to two different groups of functional, the MLPT is significantly less reliable and significantly large deviations appear. The most problematic cases involve the prediction of CH₄@HCHAB enthalpy of adsorption at the SCAN and SCAN+rVV10 levels of theory from PBE, where the deviation is larger than 8 kcal/mol.

Table 2: Enthalpies of adsorption of CH₄@HCHAB and CO₂@SiCHAB computed directly from straightforward MD (Ref. column) as well as using the MLPT method, whereby all functionals have been used as production as well as target methods. Deviations of MLPT results from the reference values (Ref. column) are given in parenthesis. All values are expressed in kcal/mol.

System	Target - MLPT	Ref.	Production - MD simulations				
			PBE	PBE+D2	SCAN	vdW-DF2	SCAN+rVV10
CH ₄ @HCHAB Exp. -4.06 ⁶⁵	PBE	-1.13	-1.18 ^(-0.05)	-1.05 ^(0.07)	1.25 ^(2.38)	-0.66 ^(0.47)	0.23 ^(1.36)
	PBE+D2	-6.08	-5.99 ^(0.09)	-6.08 ^(0.00)	-2.64 ^(3.44)	-5.10 ^(0.98)	-5.65 ^(0.43)
	SCAN	-2.60	-11.13 ^(-8.54)	-4.78 ^(-2.18)	-2.65 ^(-0.05)	-1.84 ^(0.75)	-2.37 ^(0.23)
	vdW-DF2	-5.64	-6.24 ^(-0.59)	-5.82 ^(-0.18)	-0.92 ^(4.73)	-5.53 ^(0.11)	-5.75 ^(-0.11)
	SCAN+rVV10	-4.77	-13.63 ^(-8.86)	-6.71 ^(-1.94)	-5.03 ^(-0.26)	-4.13 ^(0.64)	-4.74 ^(0.03)
CO ₂ @SiCHAB Exp. -5.02 ⁶⁶	PBE	-1.18	-1.15 ^(0.02)	-1.47 ^(-0.29)	-1.46 ^(-0.29)	-1.24 ^(-0.06)	-4.68 ^(-3.50)
	PBE+D2	-5.48	-5.61 ^(-0.14)	-5.44 ^(0.04)	-5.40 ^(0.08)	-5.60 ^(-0.12)	-7.56 ^(-2.08)
	SCAN	-2.95	-1.42 ^(1.54)	-2.74 ^(0.21)	-2.96 ^(-0.01)	-4.30 ^(-1.34)	-3.72 ^(-0.77)
	vdW-DF2	-6.93	-7.47 ^(-0.54)	-7.57 ^(-0.64)	-8.11 ^(-1.17)	-6.94 ^(-0.00)	-8.90 ^(-1.96)
	SCAN+rVV10	-7.11	-3.97 ^(3.14)	-5.52 ^(1.59)	-6.01 ^(1.10)	-7.17 ^(-0.06)	-7.09 ^(0.02)

As the enthalpies of adsorption are computed from differences of internal energies of interacting and non-interacting systems, fortuitous error cancellations might arise that could hide the real accuracy of MLPT predictions. To shed some light onto this problem, we report in **Table (3)** MLPT total ensemble energies for the individual components involved in the adsorption process (adsorbed system, zeolite alone, molecule alone). These results confirm the conclusions previously drawn from **Table (2)**, with the predictions made for the cases where the production and target methods are both from the same group of functionals (i.e., either PBE/PBE+D2/vdW-DF2 or SCAN/SCAN+rVV10) being well within the chemical accuracy.

MLPT becomes unreliable when predictions mix these two groups, with deviations that often reach several kcal/mol (these observations do not hold for the standalone CH₄ and CO₂ molecules, whose deviations are always below 0.1 kcal/mol). The worst performance is confirmed to correspond to the prediction of SCAN and SCAN+rVV10 from the PBE production trajectory of CH₄@HCHAB. For these cases, we notice that the largest deviations in the enthalpies of adsorption (>8 kcal/mol) are not only due to the low accuracy of the MLPT ensemble energy estimates for CH₄@HCHAB and HCHAB, but also to the opposite sign in deviations of predictions made for these two systems, which leads to an error accumulation when evaluating **Eq. (1)**.

While MLPT allows, in principle, for a quick evaluation of finite-temperature properties at one or more target levels of theory from a single MD production run (typically based on the most computationally inexpensive approximation), the results in **Tables (2-3)** show that such a strategy does not always allow one to achieve the required level of accuracy. Accordingly, a special care should be taken in choosing a production method suitable for the target approximation(s) of interest. The failure of MLPT in certain cases can be explained by the limitations of the thermodynamic perturbation theory (TPT) itself, rather than by

an inaccurate ML model. Indeed, if the high-probability configurational spaces of the production and target approximations do not overlap sufficiently, the TPT has low predictive power³⁵. In the most pathological cases it can happen that this overlap is so poor that in the reweighting procedure (**Eq. (2)**) only one or few individual configurations effectively contribute to the ensemble average.

Table 3: Deviations of the MLPT estimates of the target internal energies of individual systems from reference values. All values are in kcal/mol.

System	Target - MLPT	Production - MD simulations				
		PBE	PBE+D2	SCAN	vdW-DF2	SCAN+rVV10
CH ₄ @HCHAB	PBE	-0.007	0.053	-1.348	-0.237	-1.582
	PBE+D2	0.197	0.001	-0.547	0.405	-2.987
	SCAN	-4.380	-2.137	-0.029	1.497	0.204
	vdW-DF2	-0.378	0.206	0.285	0.060	-3.799
	SCAN+rVV10	-5.026	-2.036	-0.221	1.012	-0.001
CO ₂ @SiCHAB	PBE	0.014	-0.693	-2.946	-0.434	-3.689
	PBE+D2	0.245	0.041	-2.267	0.015	-1.665
	SCAN	2.249	1.244	-0.013	2.448	-0.594
	vdW-DF2	-0.053	-0.622	-4.138	-0.002	-2.122
	SCAN+rVV10	3.395	2.289	0.899	3.251	0.025
HCHAB	PBE	0.035	0.025	-3.706	-0.712	-2.953
	PBE+D2	0.054	0.000	-4.007	-0.626	-3.479
	SCAN	4.142	0.084	0.025	0.718	-0.034
	vdW-DF2	0.230	0.453	-4.407	-0.039	-3.678
	SCAN+rVV10	3.830	-0.045	0.051	0.359	-0.027
SiCHAB	PBE	-0.012	-0.380	-2.634	-0.348	-0.230
	PBE+D2	0.360	0.001	-2.337	0.145	0.353
	SCAN	0.659	1.050	0.002	3.809	0.139
	vdW-DF2	0.453	0.008	-2.972	0.001	-0.228
	SCAN+rVV10	0.246	0.745	-0.158	3.358	0.000
CH ₄	PBE	0.006	-0.047	-0.024	0.009	0.012
	PBE+D2	0.053	0.000	0.021	0.053	0.062
	SCAN	0.013	-0.039	-0.001	0.027	0.012
	vdW-DF2	-0.014	-0.067	-0.033	-0.007	-0.014
	SCAN+rVV10	0.000	-0.052	-0.013	0.014	-0.000
CO ₂	PBE	0.003	-0.018	-0.026	-0.025	0.041
	PBE+D2	0.021	-0.000	-0.007	-0.007	0.060
	SCAN	0.054	-0.018	-0.006	-0.018	0.037
	vdW-DF2	0.030	0.007	0.004	-0.001	0.070
	SCAN+rVV10	0.013	-0.049	-0.043	-0.051	0.001

In order to analyze qualitatively this behavior we consider all the production MD simulations based on the 5 different functionals. By using the t-distributed stochastic neighbor embedding (t-SNE) algorithm^{67,68} we present in **Fig. (2)** two-dimensional visualizations of the high-dimensional configurational space spanned by these trajectories (to improve the readability, figures were created using only 500 uncorrelated structures selected from each trajectory). To be consistent with the ML learning algorithm used in this study for the regression, the t-SNE approach was applied using a definition of distance D between two configurations χ^A and χ^B based on the normalized SOAP kernel K :

$$D(\chi^A, \chi^B) = (1 - K(\chi^A, \chi^B))^{\frac{1}{2}}; \quad (3)$$

this definition also inherits some of the properties of the SOAP kernel, such as the rotational and translational invariance required in materials and molecular modelling.

It can be noticed in **Fig. (2)** that for $\text{CH}_4 @ \text{HCHAB}$, $\text{CO}_2 @ \text{SiCHAB}$, HCHAB , and SiCHAB the trajectories generated by the two groups of functionals (PBE/PBE+D2/vdW-DF2 and SCAN/SCAN+rVV10) form two clusters with very limited overlap. This shows that the configurational spaces spanned by the two groups of approximations are to a large extent different, which is at the origin of the poor performance of MLPT in the cases discussed above. For the gas phase molecules CH_4 and CO_2 , the configurational space has a much simpler structure and the five different approximations produce trajectories which always largely overlap; this is also consistent with the results in **Table (3)**, where MLPT is highly accurate for all molecular energies.

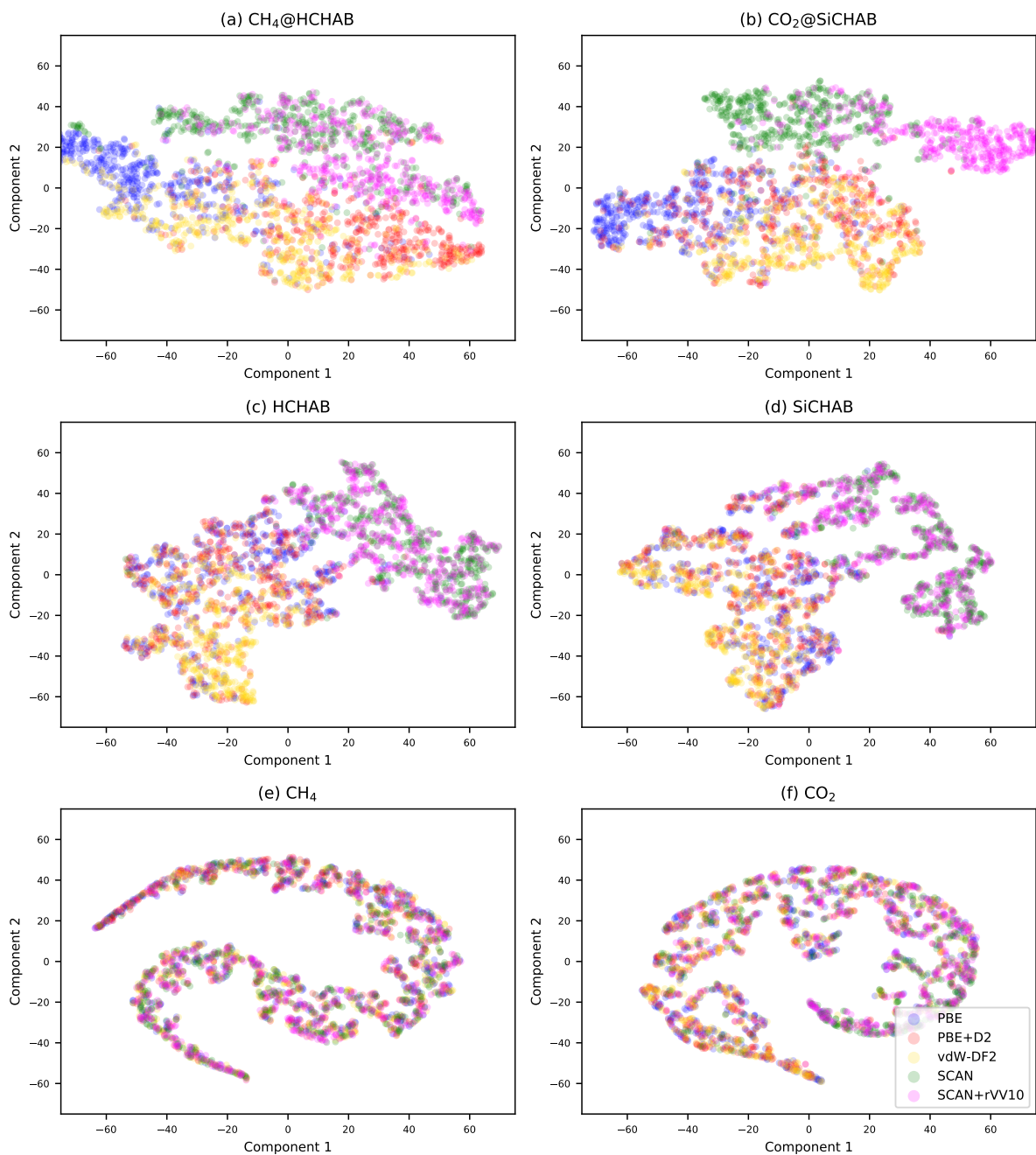


Figure 2: t-SNE representation of the configurational spaces spanned by the different functionals. This visualization is based on 500 selected configurations from each molecular dynamics trajectory. principal component of the SOAP descriptor for each 500 configurations of each functionals

The t-SNE visualization provides useful insights on the potential failures of TPT and, consequently, MLPT. However, a diagnostic approach that requires the full MD trajectories is highly impractical in reality, since the goal of MLPT is indeed to completely avoid the MD simulation at the target level of theory. In order to overcome this difficulty and introduce a tool to analyze and predict the failures of MLPT, we follow the approach introduced in Ref.²⁸ and introduce the I_w index. By considering the weight factor (w_i) in **Eq. (2)**

$$w_i = \exp(-\beta\Delta E_i) \tag{4}$$

we define $I_w = \frac{(M-N)}{M}$ where M is the total number of configurations sampled in the production run and N is the lowest integer which satisfies the condition

$$\frac{\sum_i^N w_i}{\sum_j^M w_j} \geq 0.5, \tag{5}$$

where the weights w_i have been sorted in ascending order. In practice, the I_w index reflects how many configurations contribute after the reweighting in **Eq. (2)** to half of the total statistical weight.

In the case of an extremely small overlap between configurational spaces sampled by the production and target approximations, we would have $N \approx M$ (since most weights w_i would be close to 0, N has to approach M to satisfy the condition in **Eq. (5)**) and $I_w \approx 0$. This corresponds to a significant loss in the statistical significance since the large number of configurations sampled in the production run is reduced to a few individual structures. In the opposite case of excellent overlap we would have $N \approx M/2$ and $I_w \approx 0.5$; if for example the production and target approximations provides energies that differ only by a constant we would obtain $I_w = 0.5$.

The I_w values for all systems investigated in this work are presented in **Table (4)**; in

order to simplify the analysis, we are also reporting in parenthesis the deviations of the MLPT ensemble energies with respect to the exact MD references (same as in **Table (3)**). All the the I_w values rounded to the value 0.00 actually correspond to values that are always smaller than 0.003. As expected the I_w index is equal to 0.5 when the production and target methods are the same. The values of I_w allow for an interpretation of the deviations previously reported in **Table (3)**. All the largest errors of MLPT (often significantly above chemical accuracy) correspond to $I_w = 0.00$, namely to a small correlation/overlap of production and target methods. In few cases, small deviations are found for systems with $I_w = 0.00$ (for example the MLPT evaluation of the SCAN ensemble energy from PBE+D2 for HCHAB) but these results must be considered as coincidental, whereby the reweighting of a very small number of configurations led, by chance, to a satisfactory reconstruction of the target statistical distribution.

As discussed above, the MLPT estimates become reliable for the production and target method combinations from within the two groups of functionals PBE/PBE+D2/vdW-DF2 and SCAN/SCAN+rVV10. As shown in **Table (4)** the I_w values within this two groups are all “finite” and take a value of at least 0.03. For the isolated gas phase molecules CH₄ and CO₂ we always find large values of I_w (>0.1) and consequently the errors on the energy predictions are small (within 0.18 kcal/mol). These remarks point to the fact that the I_w can be used for a qualitative *a posteriori* estimate of the reliability of MLPT. In the case of an I_w close to 0, the MLPT estimates are unpredictable and often deviate by several kcal/mol from the reference values. Non-vanishing values of I_w , ideally as close as possible to 0.5, correspond to accurate MLPT predictions. In the specific case of the systems considered here an I_w of about 0.03 already provides ensemble energies well within chemical accuracy.

Table 4: Values of the I_w index corresponding to each individual MLPT estimate of the ensemble internal energy. The values in parentheses represent the deviations in kcal/mol from the reference values obtained from straightforward MD.

System	Target - MLPT	Production - MD simulations				
		PBE	PBE+D2	SCAN	vdW-DF2	SCAN+rVV10
CH ₄ @HCHAB	PBE	0.50 ^(-0.01)	0.06 ^(0.05)	0.00 ^(-1.35)	0.03 ^(-0.24)	0.00 ^(-1.58)
	PBE+D2	0.03 ^(0.20)	0.50 ^(0.00)	0.00 ^(-0.55)	0.06 ^(0.41)	0.00 ^(-2.99)
	SCAN	0.00 ^(-4.38)	0.00 ^(-2.14)	0.50 ^(-0.03)	0.00 ^(1.50)	0.35 ^(0.20)
	vdW-DF2	0.03 ^(-0.38)	0.05 ^(0.21)	0.00 ^(0.28)	0.50 ^(0.06)	0.00 ^(-3.80)
	SCAN+rVV10	0.00 ^(-5.03)	0.00 ^(-2.04)	0.34 ^(-0.22)	0.00 ^(1.01)	0.50 ^(-0.00)
CO ₂ @SiCHAB	PBE	0.50 ^(0.01)	0.10 ^(-0.69)	0.00 ^(-2.95)	0.04 ^(-0.43)	0.00 ^(-3.69)
	PBE+D2	0.08 ^(0.24)	0.50 ^(0.04)	0.00 ^(-2.27)	0.12 ^(0.02)	0.00 ^(-1.67)
	SCAN	0.00 ^(2.25)	0.00 ^(1.24)	0.50 ^(-0.01)	0.00 ^(2.45)	0.35 ^(-0.59)
	vdW-DF2	0.03 ^(-0.05)	0.13 ^(-0.62)	0.00 ^(-4.14)	0.50 ^(-0.00)	0.00 ^(-2.12)
	SCAN+rVV10	0.00 ^(3.39)	0.00 ^(2.29)	0.32 ^(0.90)	0.00 ^(3.25)	0.50 ^(0.02)
HCHAB	PBE	0.50 ^(0.03)	0.31 ^(0.03)	0.00 ^(-3.71)	0.09 ^(-0.71)	0.00 ^(-2.95)
	PBE+D2	0.32 ^(0.05)	0.50 ^(0.00)	0.00 ^(-4.01)	0.11 ^(-0.63)	0.00 ^(-3.48)
	SCAN	0.00 ^(4.14)	0.00 ^(0.08)	0.50 ^(0.02)	0.00 ^(0.72)	0.39 ^(-0.03)
	vdW-DF2	0.08 ^(0.23)	0.11 ^(0.45)	0.00 ^(-4.41)	0.50 ^(-0.04)	0.00 ^(-3.68)
	SCAN+rVV10	0.00 ^(3.83)	0.00 ^(-0.05)	0.39 ^(0.05)	0.00 ^(0.36)	0.50 ^(-0.03)
SiCHAB	PBE	0.50 ^(-0.01)	0.36 ^(-0.38)	0.00 ^(-2.63)	0.14 ^(-0.35)	0.00 ^(-0.23)
	PBE+D2	0.35 ^(0.36)	0.50 ^(0.00)	0.00 ^(-2.34)	0.14 ^(0.14)	0.00 ^(0.35)
	SCAN	0.00 ^(0.66)	0.00 ^(1.05)	0.50 ^(0.00)	0.00 ^(3.81)	0.40 ^(0.14)
	vdW-DF2	0.13 ^(0.45)	0.15 ^(0.01)	0.00 ^(-2.97)	0.50 ^(0.00)	0.00 ^(-0.23)
	SCAN+rVV10	0.00 ^(0.25)	0.00 ^(0.74)	0.40 ^(-0.16)	0.00 ^(3.36)	0.50 ^(0.00)
CH ₄	PBE	0.50 ^(0.01)	0.46 ^(-0.05)	0.29 ^(-0.02)	0.33 ^(0.01)	0.28 ^(0.01)
	PBE+D2	0.46 ^(0.05)	0.50 ^(0.00)	0.26 ^(0.02)	0.29 ^(0.05)	0.25 ^(0.06)
	SCAN	0.29 ^(0.01)	0.26 ^(-0.04)	0.50 ^(-0.00)	0.45 ^(0.03)	0.49 ^(0.01)
	vdW-DF2	0.33 ^(-0.01)	0.30 ^(-0.07)	0.45 ^(-0.03)	0.50 ^(-0.01)	0.44 ^(-0.01)
	SCAN+rVV10	0.29 ^(0.00)	0.25 ^(-0.05)	0.49 ^(-0.01)	0.44 ^(0.01)	0.50 ^(-0.00)
CO ₂	PBE	0.50 ^(0.00)	0.50 ^(-0.02)	0.12 ^(-0.03)	0.48 ^(-0.02)	0.14 ^(0.04)
	PBE+D2	0.50 ^(0.02)	0.50 ^(-0.00)	0.11 ^(-0.01)	0.48 ^(-0.01)	0.14 ^(0.06)
	SCAN	0.11 ^(0.05)	0.12 ^(-0.02)	0.50 ^(-0.01)	0.11 ^(-0.02)	0.45 ^(0.04)
	vdW-DF2	0.48 ^(0.03)	0.48 ^(0.01)	0.11 ^(0.00)	0.50 ^(-0.00)	0.13 ^(0.07)
	SCAN+rVV10	0.14 ^(0.01)	0.15 ^(-0.05)	0.45 ^(-0.04)	0.14 ^(-0.05)	0.50 ^(0.00)

3.2 Machine learning Monte Carlo resampling

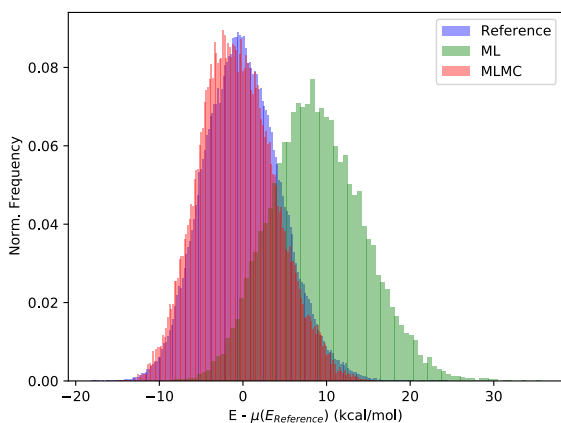
Up to this point we have discussed the origin of MLPT inaccuracies occurring in certain cases. Ideally, the production trajectory should be chosen to suit the target approximations of interest. However, this is not always possible and it is of interest to improve MLPT results also in the most pathological cases with $I_w \approx 0$. Recently, Rizzi *et al.*⁶⁹ have discussed a ML-based approach to overcome the limitations of TPT for free energy calculations in cases where there is none or very limited overlap of the configurational spaces of production and target methodologies. Following the previous approach presented by Wirnsberger *et al.*⁷⁰, Rizzi *et al.*⁶⁹ reported the use of a configurational space transformation built on a neural network model.

While this methodology is appealing, in this work we decided to pursue an approach based on the Monte Carlo resampling of the trajectory. This machine learning Monte Carlo (MLMC) method has the following advantages: The implementation is straightforward and does not require the calculation of forces, which often are not available in quantum chemical (i.e. RPA, MP2, or CC) implementations available in solid state physics codes; the same ML model of MLPT is reused and no additional calculations at the target level of theory are required; the MC resampling can be used also to verify results when a good or reasonable value of I_w is found. Finally, let us remark that the kernel methods used in our MLPT and MLMC methods typically require much smaller number of training configurations than neural networks⁷¹ used in the method of Wirnsberger *et al.*⁷⁰.

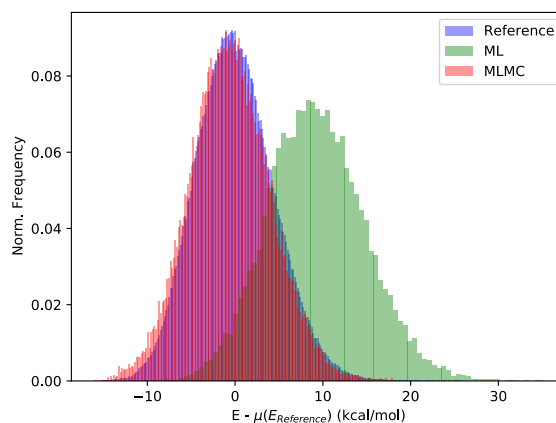
To test the MLMC approach we consider the prediction of SCAN and SCAN+rVV10 enthalpies of adsorption from PBE production calculations which showed the largest deviations between MLPT estimates and reference values. In **Fig. (3)** we show the following probability distributions of the SCAN energy determined for each zeolite and adsorbed system: the exact reference from the SCAN molecular dynamics (in blue labeled as reference); the distri-

bution of the ML predicted SCAN energies for the configurations sampled by the PBE AIMD (denoted as ML in green); the distribution of SCAN energies from the MLMC resampling (in red). The reference and ML distributions show an unsatisfactory overlap, further confirming the unsatisfactory sampling of PBE to predict SCAN properties. Since no reweighting of energies (such as in **Eq. (2)**) has been performed to generate the histograms shown in **Fig. (3)**, the ML distributions are strongly biased, and therefore deviate significantly from the reference straightforward MD results. The MLMC approach largely overcomes this issue, as it can be noticed from the good overlap of the blue and red curves. Computing the partial radial distribution function for the Si-O pairs, **Fig. (4)**, it is also evident that the MLMC generates geometries which are in a better agreement with those obtained from straightforward MD simulations with the target functional SCAN/SCAN+rVV10.

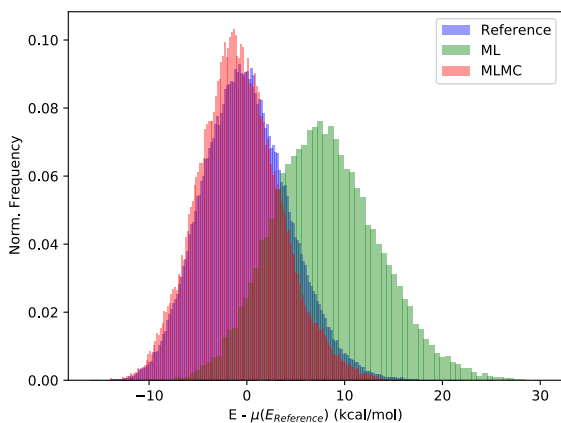
The improvement in the geometric sampling can be also demonstrated by including the MC data in the t-SNE analysis. **Fig. (5)** shows indeed that the clusters of the SCAN and SCAN+rVV10 configurations sampled by the Monte Carlo have an excellent overlap with those obtained from the reference MD simulation performed at the SCAN level. In this context it is important to emphasize again that the MLMC results are obtained without any additional explicit target level calculation.



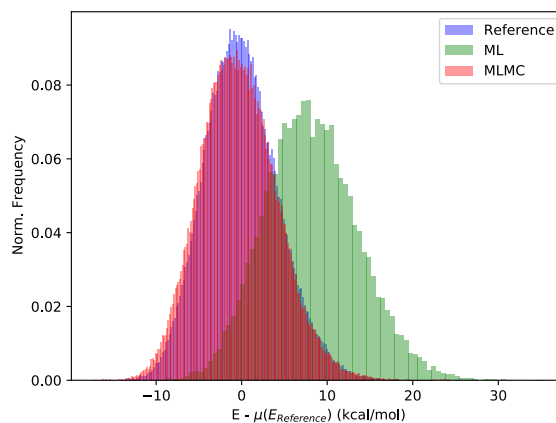
(a) CH_4 @HCHAB



(b) CO_2 @SiCHAB

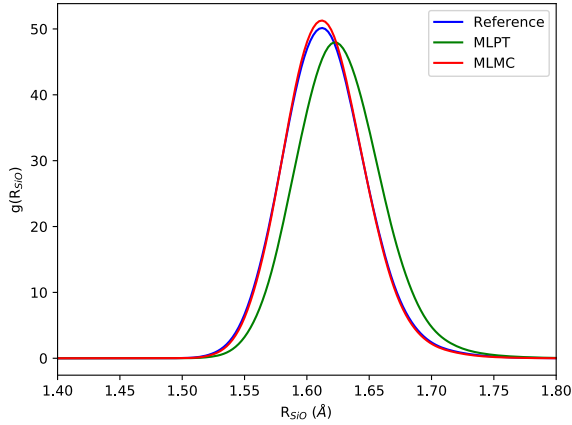


(c) HCHAB

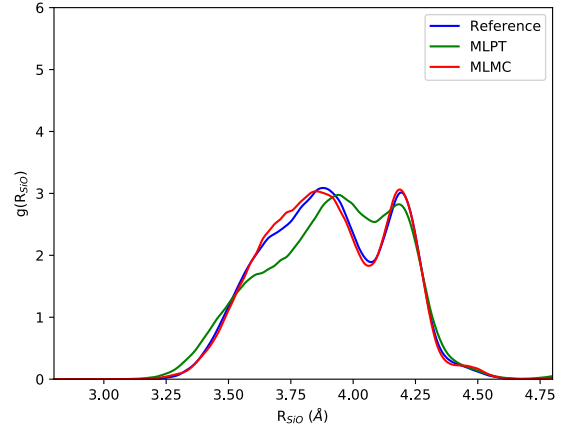


(d) SiCHAB

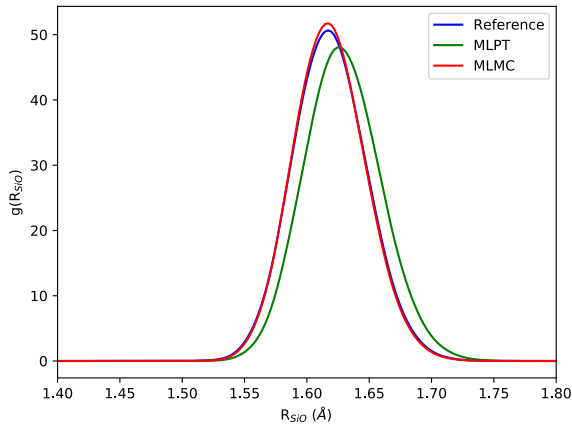
Figure 3: Distributions of deviations of SCAN energy from the average value of the corresponding reference calculation ($\mu(E_{Reference})$) obtained in three different simulations: straightforward MD calculation with the SCAN functional (blue), ML (green) and MLMC (red) with PBE production method.



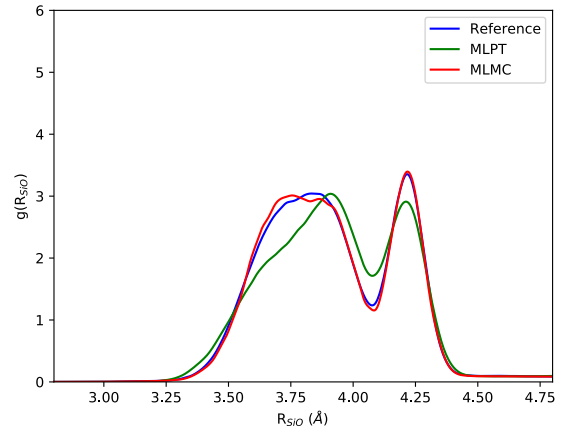
(a) 1st Shell: CH₄@HCHAB



(b) 2nd Shell: CH₄@HCHAB



(c) 1st Shell: CO₂@SiCHAB



(d) 2nd Shell: CO₂@SiCHAB

Figure 4: Radial distribution functions calculated using the SCAN functional for the first and second coordination sphere of O atoms around Si. The calculations were performed using a straightforward MD simulation performed at the SCAN level (Reference), and via the MLPT and MLMC methods based on the PBE production method.

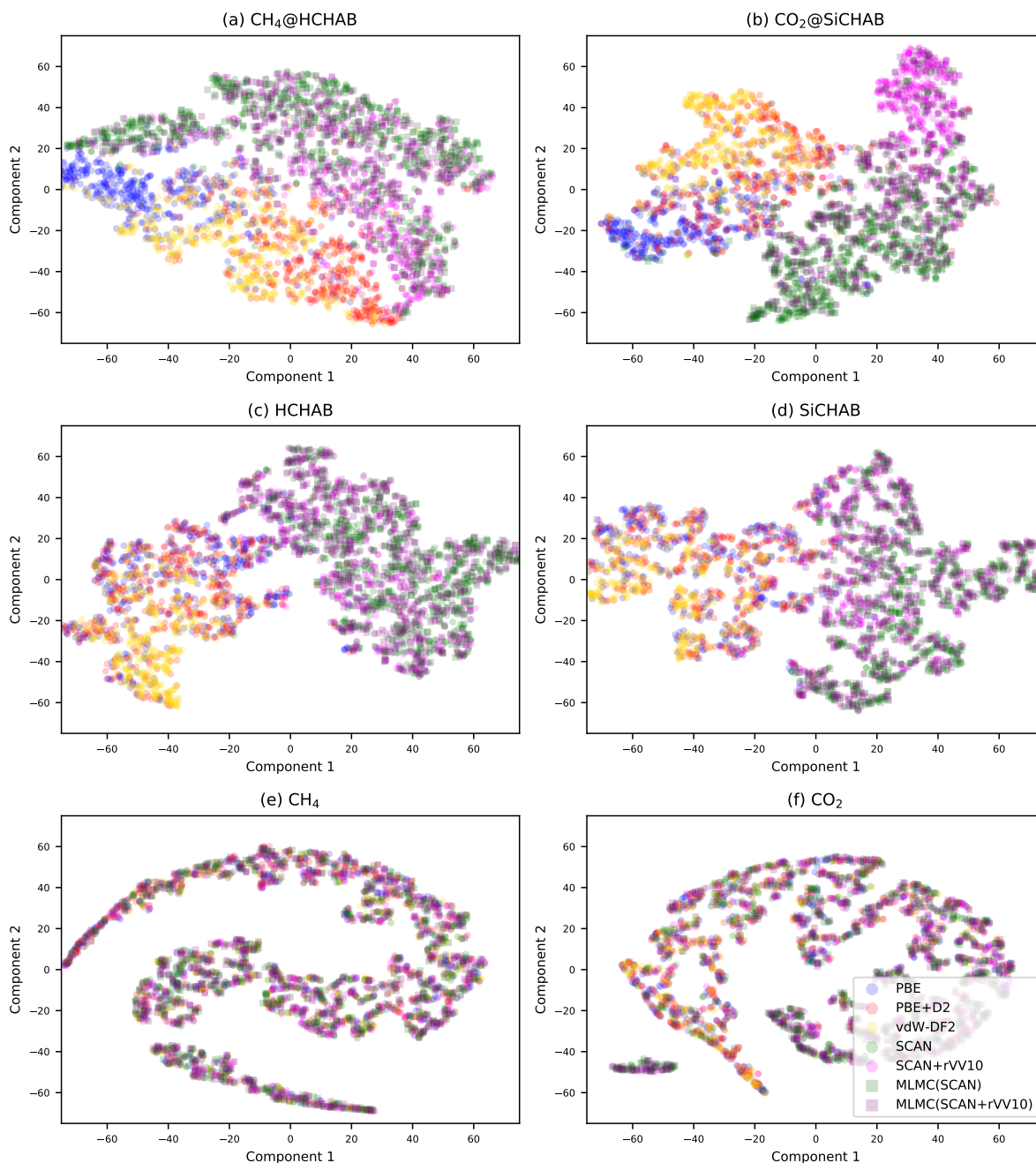


Figure 5: t-SNE representation of the configurational spaces spanned by the different functionals. This visualization is based on 500 selected configurations from each molecular dynamics trajectory and from MLMC trajectories of the SCAN (MLMC(SCAN)) and SCAN+rVV10 (MLMC(SCAN+rVV10)) functionals using PBE as production method.

We have shown insofar that the MLMC can significantly improve the sampling of the geometries at the target level. We now show in **Table (5)** the improvement in the ensemble energies. The MLMC clearly reduces error in computed internal energies of individual systems, as shown in **Table (5)**. For instance, the deviation in the internal energy of the CH₄@HCHAB at the SCAN level was reduced from -4.38 kcal/mol from MLPT with PBE production method to about -0.64 kcal/mol. Similarly, the deviations were also reduced for the predicted SCAN and SCAN+rVV10 enthalpies of adsorptions, see **Table (6)**. For CH₄@HCHAB enthalpy, for instance, the MLPT presented a deviation of -8.58 kcal/mol which reduced to only 0.12 kcal/mol when the MLMC resampling was employed.

Once again, the largest improvements have been observed for the adsorbate with substrate systems, followed by the clean zeolites, while the effect of MLPT or MLMC is negligible for the isolated molecular systems for which most of the observed deviations are close to zero and probably are related to numerical errors. In **Tables (5-6)**, all the predictions of SCAN/SCAN+rVV10 energies from PBE were significantly improved by the MLMC method. The general improvement reduced the relative internal energy deviations below 1.0 kcal/mol.

Table 5: Deviations of the SCAN and SCAN+rVV10 internal energies predicted using MLPT and MLMC from their respective reference values obtained in straightforward MD simulations (**Table (1)**). All values are expressed in kcal/mol.

System	Prediction	MLPT	MLMC
CH ₄ @HCHAB	SCAN	-4.380	-0.639
	SCAN+rVV10	-5.026	-0.858
CO ₂ @SiCHAB	SCAN	2.249	-0.564
	SCAN+rVV10	3.395	0.961
HCHAB	SCAN	4.142	-0.749
	SCAN+rVV10	3.830	-0.230
SiCHAB	SCAN	0.659	-0.345
	SCAN+rVV10	0.246	-0.267
CH ₄	SCAN	0.013	-0.011
	SCAN+rVV10	0.000	-0.014
CO ₂	SCAN	0.054	-0.005
	SCAN+rVV10	0.013	-0.058

Table 6: Experimental enthalpies of adsorption of CH₄@HCHAB and CO₂@SiCHAB and their calculated reference MLPT, and MLMC values. The deviations between the predictions and the reference MD values are given in parentheses. All values are expressed in kcal/mol.

System	Prediction	Ref.	MLPT	MLMC
CH ₄ @HCHAB	SCAN	-2.60	-11.13 ^(-8.54)	-2.48 ^(0.12)
	Exp. -4.06 ⁶⁵ SCAN+rVV10	-4.77	-13.63 ^(-8.86)	-5.38 ^(-0.61)
CO ₂ @SiCHAB	SCAN	-2.95	-1.42 ^(1.54)	-3.17 ^(-0.21)
	Exp. -5.02 ⁶⁶ SCAN+rVV10	-7.11	-3.97 ^(3.14)	-5.82 ^(1.29)

3.3 Assessing the accuracy of MLPT for the random phase approximation

In a previous work (Ref.²⁷) some of us applied MLPT to compute enthalpies of adsorption at the RPA level of theory. Beyond the two systems studied in this work, also CH₄@CHAB and CO₂@HCHAB were considered in this previous paper. The RPA enthalpies of adsorption showed an excellent agreement with experiment and for the molecules adsorbed in HCHAB zeolite a significant improvement with respect to the production method (PBE+D2) was found (the results for ensemble energies and enthalpies of adsorption will not be repeated here, where we will rather discuss their reliability). Because of the high computational cost involved in the RPA calculations in this case, it is not possible to produce reference trajectories and use them to repeat some of the previous analysis (indeed MLPT is meant to make possible finite-temperature calculations involving computationally expensive approximations).

However, the I_w index can be straightforwardly obtained and we present its values in **Table (7)**. This type of analysis, which we did not develop in the original paper, Ref.²⁷, shows that a good performance of MLPT should be expected, as the I_w coefficient takes for all systems values above 0.1. While not strictly necessary, the accuracy can be further confirmed by applying MLMC, which requires several additional production level calculations but avoids completely the highly expensive RPA calculations. To this purpose we consider a subset of the systems in **Table (7)** (the two adsorbed systems with the lowest I_w and the two zeolites). With respect to the MLPT values reported in Ref.²⁷, the MLMC results present only small deviations: -0.21 kcal/mol for CO₂@HCHAB, -0.48 kcal/mol for CH₄@HCHAB, -0.65 kcal/mol for HCHAB, and -0.05 kcal/mol for SiCHAB. Keeping in mind that also statistical errors should be considered (the standard error in the MC sampling is about 0.3 kcal/mol), we conclude that the agreement between MLPT and MLMC results is very good from which we deduce that PBE+D2 is a suitable production method for the RPA target

level calculations and that the Monte Carlo resampling of the MLPT results is not strictly necessary.

Table 7: Values of the I_w index corresponding to the MLPT predictions of RPA energies from PBE+D2 trajectories for the different systems considered in Ref. ²⁷.

System	RPA
CH ₄ @HCHAB	0.13
CO ₂ @HCHAB	0.21
CH ₄ @SiCHAB	0.26
CO ₂ @SiCHAB	0.27
HCHAB	0.28
SiCHAB	0.32

4 Conclusions

We assessed the accuracy of the machine learning thermodynamic perturbation theory approach by computing enthalpies of adsorption of molecules in zeolites. By considering a set of five DFT functionals with different characteristics, MLPT estimates are compared to reference results produced from full MD simulations. The largest deviations are found when the configurational space accessible to the target level has a small overlap with that sampled by the production method. Even when an exact reference result is not available, the most problematic cases can be detected by using a diagnostic test, the I_w index. In these cases the results can be significantly improved by coupling the Monte Carlo approach to the MLPT model to resample the configurational space at the target level of theory which is, however, performed at the cost of the production method.

Finally, the analysis is extended to some recently published MLPT results that used the RPA as target approximation²⁷; in this case the high computational cost of the RPA makes the generation of exact reference ensemble energies and enthalpies completely unpractical. The application of the I_w diagnostic test and of the MC resampling highlights the full reliability of those previous results, which were based on PBE+D2 production MD.

The main advantage of the MLPT approach stands in the possibility of evaluating finite temperature properties at a certain target level of theory by performing only a minimal number of single-point calculations. Additionally, MLPT is also suitable for approximations where the computation of gradients is not available or adds a significant computational cost³⁰. This approach opens the possibility of systematically applying high-accuracy/high-cost *ab initio* methodologies to achieve a new level of predictive power in materials simulations.

Acknowledgement

This work was supported through the COMETE project (COncEption in silico de Matériaux pour l'Environnement et l'Energie) co-funded by the European Union under the program “FEDER-FSE Lorraine et Massif des Vosges 2014-2020”. This work was granted access to the HPC resources of TGCC under the allocations 2020- A0080810433 and 2021-A0100810433 by GENCI -EDARI project. TB acknowledges support from the Slovak Research and Development Agency under the contracts No. VEGA-1/0777/19 and APVV-20-0127.

References

- (1) Møller, C.; Plesset, M. S. Note on an Approximation Treatment for Many-Electron Systems. *Phys. Rev.* **1934**, *46*, 618–622, DOI: 10.1103/PhysRev.46.618.
- (2) Bartlett, R. J.; Musiał, M. Coupled-cluster theory in quantum chemistry. *Rev. Mod. Phys.* **2007**, *79*, 291–352, DOI: 10.1103/RevModPhys.79.291.
- (3) Pisani, C.; Maschio, L.; Casassa, S.; Halo, M.; Schütz, M.; Usvyat, D. Periodic local MP2 method for the study of electronic correlation in crystals: Theory and preliminary applications. *J. Comp. Chem.* **2008**, *29*, 2113–2124, DOI: 10.1002/jcc.20975.
- (4) Marsman, M.; Grüneis, A.; Paier, J.; Kresse, G. Second-order Møller–Plesset perturbation theory applied to extended systems. I. Within the projector-augmented-wave formalism using a plane wave basis set. *J. Chem. Phys.* **2009**, *130*, 184103, DOI: 10.1063/1.3126249.
- (5) Del Ben, M.; Hutter, J.; VandeVondele, J. Second-Order Møller–Plesset Perturbation Theory in the Condensed Phase: An Efficient and Massively Parallel Gaussian and Plane Waves Approach. *J. Chem. Theory Comput.* **2012**, *8*, 4177–4188, DOI: 10.1021/ct300531w.
- (6) Booth, G. H.; Grüneis, A.; Kresse, G.; Alavi, A. Towards an exact description of electronic wavefunctions in real solids. *Nature* **2013**, *493*, 365–370, DOI: 10.1038/nature11770.
- (7) Dixit, A.; Claudot, J.; Lebègue, S.; Rocca, D. Communication: A novel implementation to compute MP2 correlation energies without basis set superposition errors and complete basis set extrapolation. *J. Chem. Phys.* **2017**, *146*, 211102, DOI: 10.1063/1.4985096.

- (8) Bohm, D.; Pines, D. A Collective Description of Electron Interactions: III. Coulomb Interactions in a Degenerate Electron Gas. *Phys. Rev.* **1953**, *92*, 609–625, DOI: 10.1103/PhysRev.92.609.
- (9) Gell-Mann, M.; Brueckner, K. A. Correlation Energy of an Electron Gas at High Density. *Phys. Rev.* **1957**, *106*, 364–368, DOI: 10.1103/PhysRev.106.364.
- (10) Langreth, D.; Perdew, J. The exchange-correlation energy of a metallic surface. *Solid State Commun.* **1975**, *17*, 1425–1429, DOI: 10.1016/0038-1098(75)90618-3.
- (11) Dobson, J. F.; Wang, J. Successful Test of a Seamless van der Waals Density Functional. *Phys. Rev. Lett.* **1999**, *82*, 2123–2126, DOI: 10.1103/PhysRevLett.82.2123.
- (12) Furche, F. Molecular tests of the random phase approximation to the exchange-correlation energy functional. *Phys. Rev. B* **2001**, *64*, 195120, DOI: 10.1103/PhysRevB.64.195120.
- (13) Harl, J.; Kresse, G. Cohesive energy curves for noble gas solids calculated by adiabatic connection fluctuation-dissipation theory. *Phys. Rev. B* **2008**, *77*, 045136, DOI: 10.1103/PhysRevB.77.045136.
- (14) Lu, D.; Li, Y.; Rocca, D.; Galli, G. Ab initio Calculation of van der Waals Bonded Molecular Crystals. *Phys. Rev. Lett.* **2009**, *102*, 206411, DOI: 10.1103/PhysRevLett.102.206411.
- (15) Grüneis, A.; Marsman, M.; Harl, J.; Schimka, L.; Kresse, G. Making the random phase approximation to electronic correlation accurate. *J. Chem. Phys.* **2009**, *131*, 154115, DOI: 10.1063/1.3250347.
- (16) Olsen, T.; Thygesen, K. S. Extending the random-phase approximation for electronic correlation energies: The renormalized adiabatic local density approximation. *Phys. Rev. B* **2012**, *86*, 081103, DOI: 10.1103/PhysRevB.86.081103.

- (17) Bates, J. E.; Furche, F. Communication: Random phase approximation renormalized many-body perturbation theory. *J. Chem. Phys.* **2013**, *139*, 171103, DOI: 10.1063/1.4827254.
- (18) Colonna, N.; Hellgren, M.; de Gironcoli, S. Correlation energy within exact-exchange adiabatic connection fluctuation-dissipation theory: Systematic development and simple approximations. *Phys. Rev. B* **2014**, *90*, 125150, DOI: 10.1103/PhysRevB.90.125150.
- (19) Dixit, A.; Ángyán, J. G.; Rocca, D. Improving the accuracy of ground-state correlation energies within a plane-wave basis set: The electron-hole exchange kernel. *J. Chem. Phys.* **2016**, *145*, 104105, DOI: 10.1063/1.4962352.
- (20) Dixit, A.; Claudot, J.; Lebègue, S.; Rocca, D. Improving the Efficiency of Beyond-RPA Methods within the Dielectric Matrix Formulation: Algorithms and Applications to the A24 and S22 Test Sets. *J. Chem. Theory Comput.* **2017**, *13*, 5432–5442, DOI: 10.1021/acs.jctc.7b00837.
- (21) Hellgren, M.; Colonna, N.; de Gironcoli, S. Beyond the random phase approximation with a local exchange vertex. *Phys. Rev. B* **2018**, *98*, 045117, DOI: 10.1103/PhysRevB.98.045117.
- (22) Behler, J.; Parrinello, M. Generalized Neural-Network Representation of High-Dimensional Potential-Energy Surfaces. *Phys. Rev. Lett.* **2007**, *98*, 146401, DOI: 10.1103/PhysRevLett.98.146401.
- (23) Chmiela, S.; Tkatchenko, A.; Sauceda, H. E.; Poltavsky, I.; Schütt, K. T.; Müller, K.-R. Machine learning of accurate energy-conserving molecular force fields. *Sci. Adv.* **2017**, *3*, DOI: 10.1126/sciadv.1603015.
- (24) Chmiela, S.; Sauceda, H. E.; Müller, K.-R.; Tkatchenko, A. Towards exact molecular

- dynamics simulations with machine-learned force fields. *Nat. Commun.* **2018**, *9*, 3887, DOI: 10.1038/s41467-018-06169-2.
- (25) Zhang, L.; Han, J.; Wang, H.; Car, R.; E, W. Deep Potential Molecular Dynamics: A Scalable Model with the Accuracy of Quantum Mechanics. *Phys. Rev. Lett.* **2018**, *120*, 143001, DOI: 10.1103/PhysRevLett.120.143001.
- (26) Behler, J. Perspective: Machine learning potentials for atomistic simulations. *J. Chem. Phys.* **2016**, *145*, 170901, DOI: 10.1063/1.4966192.
- (27) Chehaibou, B.; Badawi, M.; Bučko, T.; Bazhurov, T.; Rocca, D. Computing RPA Adsorption Enthalpies by Machine Learning Thermodynamic Perturbation Theory. *J. Chem. Theory Comput.* **2019**, *15*, 6333–6342, DOI: 10.1021/acs.jctc.9b00782.
- (28) Bučko, T.; Gešvandtnerová, M.; Rocca, D. Ab Initio Calculations of Free Energy of Activation at Multiple Electronic Structure Levels Made Affordable: An Effective Combination of Perturbation Theory and Machine Learning. *J. Chem. Theory Comput.* **2020**, *16*, 6049–6060, DOI: 10.1021/acs.jctc.0c00486.
- (29) Gešvandtnerová, M.; Rocca, D.; Bučko, T. Methanol carbonylation over acid mordenite: Insights from ab initio molecular dynamics and machine learning thermodynamic perturbation theory. *J. Catal.* **2021**, *396*, 166–178, DOI: 10.1016/j.jcat.2021.02.011.
- (30) Ramberger, B.; Schäfer, T.; Kresse, G. Analytic interatomic forces in the random phase approximation. *Phys. Rev. Lett.* **2017**, *118*, 106403, DOI: 10.1103/PhysRevLett.118.106403.
- (31) Grimme, S. Semiempirical GGA-type density functional constructed with a long-range dispersion correction. *J. Comp. Chem.* **2006**, *27*, 1787–1799, DOI: 10.1002/jcc.20495.
- (32) Bučko, T.; Hafner, J.; Lebègue, S.; Angyan, J. G. Improved Description of the Structure

- of Molecular and Layered Crystals: Ab Initio DFT Calculations with van der Waals Corrections. *J. Phys. Chem. A* **2010**, *114*, 11814–11824, DOI: 10.1021/jp106469x.
- (33) Ramakrishnan, R.; Dral, P. O.; Rupp, M.; von Lilienfeld, O. A. Big Data Meets Quantum Chemistry Approximations: The Δ -Machine Learning Approach. *J. Chem. Theory Comput.* **2015**, *11*, 2087–2096, DOI: 10.1021/acs.jctc.5b00099.
- (34) Chipot, C.; Pohorille, A. *Free energy calculations: Theory and Applications in Chemistry and Biology*; Springer, 2016.
- (35) Pohorille, A.; Jarzynski, C.; Chipot, C. Good Practices in Free-Energy Calculations. *J. Phys. Chem. B* **2010**, *114*, 10235–10253, DOI: 10.1021/jp102971x.
- (36) Rocca, D.; Dixit, A.; Badawi, M.; Lebègue, S.; Gould, T.; Bučko, T. Bridging molecular dynamics and correlated wave-function methods for accurate finite-temperature properties. *Phys. Rev. Mater.* **2019**, *3*, 040801, DOI: 10.1103/PhysRevMaterials.3.040801.
- (37) Adil, K.; Belmabkhout, Y.; Pillai, R. S.; Cadiau, A.; Bhatt, P. M.; Assen, A. H.; Maurin, G.; Eddaoudi, M. Gas/vapour separation using ultra-microporous metal–organic frameworks: insights into the structure/separation relationship. *Chem. Soc. Rev* **2017**, *46*, 3402–3430, DOI: 10.1039/C7CS00153C.
- (38) Khalil, I.; Jabraoui, H.; Lebègue, S.; Kim, W. J.; Aguilera, L.-J.; Thomas, K.; Maugé, F.; Badawi, M. Biofuel purification: Coupling experimental and theoretical investigations for efficient separation of phenol from aromatics by zeolites. *Chem. Eng. J.* **2020**, *402*, 126264, DOI: 10.1016/j.cej.2020.126264.
- (39) Chibani, S.; Chebbi, M.; Lebègue, S.; Bučko, T.; Badawi, M. A DFT investigation of the adsorption of iodine compounds and water in H-, Na-, Ag-, and Cu- mordenite. *J. Chem. Phys.* **2016**, *144*, 244705, DOI: 10.1063/1.4954659.

- (40) Hessou, E. P.; Jabraoui, H.; Khalil, I.; Dziurla, M.-A.; Badawi, M. Ab initio screening of zeolite Y formulations for efficient adsorption of thiophene in presence of benzene. *Appl. Surf. Sci.* **2021**, *541*, 148515, DOI: 10.1016/j.apsusc.2020.148515.
- (41) Perdew, J. P.; Burke, K.; Ernzerhof, M. Generalized Gradient Approximation Made Simple. *Phys. Rev. Lett.* **1996**, *77*, 3865–3868, DOI: 10.1103/PhysRevLett.77.3865.
- (42) Sun, J.; Ruzsinszky, A.; Perdew, J. Strongly Constrained and Appropriately Normed Semilocal Density Functional. *Phys. Rev. Lett.* **2015**, *115*, 036402, DOI: 10.1103/PhysRevLett.115.036402.
- (43) Sun, J.; Remsing, R. C.; Zhang, Y.; Sun, Z.; Ruzsinszky, A.; Peng, H.; Yang, Z.; Paul, A.; Waghmare, U.; Wu, X.; Klein, M. L.; Perdew, J. P. Accurate first-principles structures and energies of diversely bonded systems from an efficient density functional. *Nat. Chem.* **2016**, *8*, 831–836, DOI: 10.1038/nchem.2535.
- (44) Román-Pérez, G.; Soler, J. M. Efficient Implementation of a van der Waals Density Functional: Application to Double-Wall Carbon Nanotubes. *Phys. Rev. Lett.* **2009**, *103*, 096102, DOI: 10.1103/PhysRevLett.103.096102.
- (45) Dion, M.; Rydberg, H.; Schröder, E.; Langreth, D. C.; Lundqvist, B. I. Van der Waals Density Functional for General Geometries. *Phys. Rev. Lett.* **2004**, *92*, 246401, DOI: 10.1103/PhysRevLett.92.246401.
- (46) Peng, H.; Yang, Z.-H.; Perdew, J. P.; Sun, J. Versatile van der Waals Density Functional Based on a Meta-Generalized Gradient Approximation. *Phys. Rev. X* **2016**, *6*, 041005, DOI: 10.1103/PhysRevX.6.041005.
- (47) Kresse, G.; Hafner, J. Ab initio molecular dynamics for liquid metals. *Phys. Rev. B* **1993**, *47*, 558–561, DOI: 10.1103/PhysRevB.47.558.

- (48) Kresse, G.; Furthmüller, J. Efficient iterative schemes for ab initio total-energy calculations using a plane-wave basis set. *Phys. Rev. B* **1996**, *54*, 11169–11186, DOI: 10.1103/PhysRevB.54.11169.
- (49) Kresse, G.; Furthmüller, J. Efficiency of ab-initio total energy calculations for metals and semiconductors using a plane-wave basis set. *Comp. Mater. Sci.* **1996**, *6*, 15–50, DOI: 10.1016/0927-0256(96)00008-0.
- (50) Andersen, H. C. Molecular dynamics simulations at constant pressure and/or temperature. *J. Chem. Phys.* **1980**, *72*, 2384–2393, DOI: 10.1063/1.439486.
- (51) Schiferl, S. K.; Wallace, D. C. Statistical errors in molecular dynamics averages. *J. Chem. Phys.* **1985**, *83*, 5203–5209, DOI: 10.1063/1.449733.
- (52) Kresse, G.; Joubert, D. From ultrasoft pseudopotentials to the projector augmented-wave method. *Phys. Rev. B* **1999**, *59*, 1758–1775, DOI: 10.1103/PhysRevB.59.1758.
- (53) Deringer, V. L.; Bernstein, N.; Csányi, G.; Ben Mahmoud, C.; Ceriotti, M.; Wilson, M.; Drabold, D. A.; Elliott, S. R. Origins of structural and electronic transitions in disordered silicon. *Nature* **2021**, *589*, 59–64, DOI: 10.1038/s41586-020-03072-z.
- (54) Bartók, A. P.; Kondor, R.; Csányi, G. On representing chemical environments. *Phys. Rev. B* **2013**, *87*, 184115, DOI: 10.1103/PhysRevB.87.184115.
- (55) Himanen, L.; Jäger, M. O.; Morooka, E. V.; Federici Canova, F.; Ranawat, Y. S.; Gao, D. Z.; Rinke, P.; Foster, A. S. Dscribe: Library of descriptors for machine learning in materials science. *Comput. Phys. Commun.* **2020**, *247*, 106949, DOI: 10.1016/j.cpc.2019.106949.
- (56) Behler, J. Atom-centered symmetry functions for constructing high-dimensional neural network potentials. *J. Chem. Phys.* **2011**, *134*, 074106, DOI: 10.1063/1.3553717.

- (57) Huo, H.; Rupp, M. Unified Representation of Molecules and Crystals for Machine Learning. *arXiv:1704.06439 [physics.chem-ph]* **2018**,
- (58) Casier, B.; Chagas da Silva, M.; Badawi, M.; Pascale, F.; Bučko, T.; Lebègue, S.; Rocca, D. Hybrid localized graph kernel for machine learning energy-related properties of molecules and solids. *J. Comp. Chem.* **2021**, *42*, 1390–1401, DOI: 10.1002/jcc.26550.
- (59) Stuke, A.; Todorović, M.; Rupp, M.; Kunkel, C.; Ghosh, K.; Himanen, L.; Rinke, P. Chemical diversity in molecular orbital energy predictions with kernel ridge regression. *J. Chem. Phys.* **2019**, *150*, 204121, DOI: 10.1063/1.5086105.
- (60) Pedregosa, F. et al. Scikit-learn: Machine Learning in Python. *J. Mach. Learn. Res.* **2011**, *12*, 2825–2830.
- (61) Paquet, E.; Viktor, H. L. Molecular Dynamics, Monte Carlo Simulations, and Langevin Dynamics: A Computational Review. *Biomed Res. Int.* **2015**, *2015*, 1–18, DOI: 10.1155/2015/183918.
- (62) Kremer, K.; Grest, G. S. Monte Carlo and molecular dynamics simulations of polymers. *Phys. Scr.* **1991**, *T35*, 61–65, DOI: 10.1088/0031-8949/1991/T35/013.
- (63) Meimaroglou, D.; Kiparissides, C. Review of Monte Carlo Methods for the Prediction of Distributed Molecular and Morphological Polymer Properties. *Ind. Eng. Chem. Res.* **2014**, *53*, 8963–8979, DOI: 10.1021/ie4033044.
- (64) Betancourt, M. The Convergence of Markov Chain Monte Carlo Methods: From the Metropolis Method to Hamiltonian Monte Carlo. *Ann. Phys.* **2019**, *531*, 1700214, DOI: 10.1002/andp.201700214.
- (65) Piccini, G.; Alessio, M.; Sauer, J.; Zhi, Y.; Liu, Y.; Kolvenbach, R.; Jentys, A.; Lercher, J. A. Accurate Adsorption Thermodynamics of Small Alkanes in Zeolites. Ab

- initio Theory and Experiment for H-Chabazite. *J. Phys. Chem. C* **2015**, *119*, 6128–6137, DOI: 10.1021/acs.jpcc.5b01739.
- (66) Maghsoudi, H.; Soltanieh, M.; Bozorgzadeh, H.; Mohamadalizadeh, A. Adsorption isotherms and ideal selectivities of hydrogen sulfide and carbon dioxide over methane for the Si-CHA zeolite: comparison of carbon dioxide and methane adsorption with the all-silica DD3R zeolite. *Adsorption* **2013**, *19*, 1045–1053, DOI: 10.1007/s10450-013-9528-1.
- (67) Van Der Maaten, L.; Hinton, G. *Visualizing Data using t-SNE*; 2008; Vol. 9; pp 2579–2605.
- (68) De, S.; Bartók, A. P.; Csányi, G.; Ceriotti, M. Comparing molecules and solids across structural and alchemical space. *Phys. Chem. Chem. Phys.* **2016**, *18*, 13754–13769, DOI: 10.1039/C6CP00415F.
- (69) Rizzi, A.; Carloni, P.; Parrinello, M. Targeted Free Energy Perturbation Revisited: Accurate Free Energies from Mapped Reference Potentials. *J. Phys. Chem. Lett.* **2021**, 9449–9454, DOI: 10.1021/acs.jpcllett.1c02135.
- (70) Wirnsberger, P.; Ballard, A. J.; Papamakarios, G.; Abercrombie, S.; Racanière, S.; Pritzel, A.; Jimenez Rezende, D.; Blundell, C. Targeted free energy estimation via learned mappings. *J. Chem. Phys.* **2020**, *153*, 144112, DOI: 10.1063/5.0018903.
- (71) Jablonka, K. M.; Ongari, D.; Moosavi, S. M.; Smit, B. Big-Data Science in Porous Materials: Materials Genomics and Machine Learning. *Chem. Rev.* **2020**, *120*, 8066–8129, DOI: 10.1021/acs.chemrev.0c00004.

Graphical TOC Entry

